NeuroImage 223 (2020) 117270

Contents lists available at ScienceDirect

NeuroImage

journal homepage: www.elsevier.com/locate/neuroimage

Association of dopamine $D_{2/3}$ receptor binding potential measured using PET and [^{11}C]-(+)-PHNO with post-mortem $DRD_{2/3}$ gene expression in the human brain

Arkadiusz Komorowski[a,1], Ana Weidenauer[a,1], Matej Murgaš[a], Ulrich Sauerzopf[a], Wolfgang Wadsak[b,c], Markus Mitterhauser[b,d], Martin Bauer[e], Marcus Hacker[b], Nicole Praschak-Rieder[a], Siegfried Kasper[f], Rupert Lanzenberger[a,*], Matthäus Willeit[a]

[a] Department of Psychiatry and Psychotherapy, Division of General Psychiatry, Medical University of Vienna, Währinger Gürtel 18-20, 1090 Vienna, Austria
[b] Department of Biomedical Imaging and Image-guided Therapy, Division of Nuclear Medicine, Medical University of Vienna, Vienna, Austria
[c] Center for Biomarker Research in Medicine (CBmed), Graz, Austria
[d] Ludwig Boltzmann Institute for Applied Diagnostics, Vienna, Austria
[e] Department of Clinical Pharmacology, Medical University of Vienna, Vienna, Austria
[f] Center for Brain Research, Medical University of Vienna, Vienna, Austria

ARTICLE INFO

Key words:
Dopamine
$D_{2/3}$
[^{11}C]-(+)-PHNO
mRNA

ABSTRACT

Open access post-mortem transcriptome atlases such as the Allen Human Brain Atlas (AHBA) can inform us about mRNA expression of numerous proteins of interest across the whole brain, while in vivo protein binding in the human brain can be quantified by means of neuroreceptor positron emission tomography (PET). By combining both modalities, the association between regional gene expression and receptor distribution in the living brain can be approximated. Here, we compare the characteristics of D_2 and D_3 dopamine receptor distribution by applying the dopamine $D_{2/3}$ receptor agonist radioligand [^{11}C]-(+)-PHNO and human gene expression data. Since [^{11}C]-(+)-PHNO has a higher affinity for D_3 compared to D_2 receptors, we hypothesized that there is a stronger relationship between $D_{2/3}$ non-displaceable binding potentials (BP_{ND}) and D_3 mRNA expression. To investigate the relationship between $D_{2/3}$ BP_{ND} and mRNA expression of DRD2 and DRD3 we performed [^{11}C]-(+)-PHNO PET scans in 27 healthy subjects (12 females) and extracted gene expression data from the AHBA. We also calculated D_2/D_3 mRNA expression ratios to imitate the mixed $D_{2/3}$ signal of [^{11}C]-(+)-PHNO. In accordance with our a priori hypothesis, a strong correlation between [^{11}C]-(+)-PHNO and DRD3 expression was found. However, there was no significant correlation with DRD2 expression. Calculated D_2/D_3 mRNA expression ratios also showed a positive correlation with [^{11}C]-(+)-PHNO binding, reflecting the mixed $D_{2/3}$ signal of the radioligand. Our study supports the usefulness of combining gene expression data from open access brain atlases with in vivo imaging data in order to gain more detailed knowledge on neurotransmitter signaling.

1. Introduction

Increasingly sophisticated neuroimaging methods and data-sharing initiatives have furthered the understanding of human brain function. Using the Allen Human Brain Atlas (AHBA; http://human.brain-map.org) (Hawrylycz et al., 2012), numerous studies investigating the relationship between structural and functional brain parameters and the transcriptome were published recently (Burt, 2018; Goel et al., 2014; Richiardi et al., 2015; Shin et al., 2017). Several authors showed close associations of gene expression levels with in vivo protein densities, mainly focusing on serotonergic neurotransmitter receptors (Komorowski et al., 2017; Rizzo et al., 2016; Unterholzner et al., 2020). Similar to the serotonergic system, dopamine signaling is mediated through G-protein-coupled receptors and plays a crucial role in physiologic and pathologic processes in humans, including neuropsychiatric conditions (Beaulieu and Gainetdinov, 2011). To identify pathophysiological mechanisms within the dopamine system, different neuroimaging modalities including high-resolution whole-brain transcriptome maps (Gryglewski et al., 2018) and positron emission tomography (PET) imaging data of dopamine receptors can be integrated, extending previous studies on dopamine receptors. Labelled with carbon-11, (+)-4-propyl-3,4,4a,5,6,10b-hexahydro-2H-naphtho[1,2-b][1,4]oxazin-9-ol ([^{11}C]-(+)-PHNO) (Wilson et al., 2005), a radioligand with full agonistic properties at dopamine $D_{2/3}$ receptors (Brown et al., 1997) offers an excellent signal-to-noise (SNR) ratio and favourable kinetics for PET imaging in humans (Ginovart et al.,

* Corresponding author.
E-mail address: rupert.lanzenberger@meduniwien.ac.at (R. Lanzenberger).
[1] Contributed equally

https://doi.org/10.1016/j.neuroimage.2020.117270
Received 5 May 2020; Received in revised form 12 August 2020; Accepted 12 August 2020
Available online 17 August 2020

2007; Jensen et al., 2007). Many studies using [^{11}C]-(+)-PHNO have focused on schizophrenia (Graff-Guerrero et al., 2009; Mizrahi et al., 2012; Mizrahi et al., 2011; Mizrahi et al., 2014; Suridjan et al., 2013; Weidenauer et al., 2020), or substance use disorders (Boileau et al., 2015; Boileau et al., 2012; Payer et al., 2014; Worhunsky et al., 2017). Applying PET, several approaches have been described to determine the relative affinity of [^{11}C]-(+)-PHNO as well as the regionally distinctive topology of D_2 compared to D_3 receptors, including pharmacological and animal studies (Graff-Guerrero et al., 2009). Depending on G-protein binding, the dopamine D_2 receptor occurs in an interconvertible high- and low-affinity state (D_2^{high} vs. D_2^{low}) towards its natural agonist dopamine, with the high-affinity state being the functionally active one (George et al., 1985). In contrast, G-protein binding has comparably little influence on the affinity of D_3 receptors for dopamine (Sokoloff et al., 1992). Thus, D_3 receptors are assumed to be "locked" in the high-affinity state, affecting binding of $D_{2/3}$ radiotracers with a yet unknown fraction. It is well supported that [^{11}C]-(+)-PHNO binds more to D_2^{high} than to D_2^{low} (Nobrega and Seeman, 1994; Seeman et al., 1993), and PET imaging studies in non-human primates indicate that in vivo [^{11}C]-(+)-PHNO has a 25-48 fold higher affinity for D_3 over D_2 receptors (Gallezot et al., 2012). Being easily displaced by endogenous dopamine, [^{11}C]-(+)-PHNO is a useful tool for challenge studies (Ginovart et al., 2006; Weidenauer et al., 2020; Willeit et al., 2008; Willeit et al., 2006). Still, although several studies addressed this issue in animals and humans (Graff-Guerrero et al., 2010; Rabiner et al., 2009; Searle et al., 2010; Seeman et al., 2007; Tziortzi et al., 2011), the relative contribution of extracellular dopamine, D_2^{high}, D_2^{low} and D_3 binding to the [^{11}C]-(+)-PHNO overall signal is insufficiently understood to this day.

In this study, we aimed to contribute to the disentangling of the [^{11}C]-(+)-PHNO PET signal into the respective fractions of D_2 vs. D_3 receptors by relating subcortical non-displaceable binding potential (BP_{ND}) values of healthy human subjects to gene expression data obtained from the AHBA and interpolated transcriptome maps according to Gryglewski et al. (Gryglewski et al., 2018).

2. Methods

2.1. Participants

Imaging data were acquired in a larger study investigating dopamine release in healthy subjects and patients with schizophrenia (Weidenauer et al., 2020) (Clinical Trial Registry: EUDRACT 2010-019586-29). Here, analysis was restricted to healthy participants. All study procedures were approved by the Ethics Committee of the Medical University of Vienna and pertinent federal regulatory authorities. After being informed on study procedures and study-related risks, participants gave written informed consent. Subjects were only included if they were free of medical or neurological disorders and if laboratory or urine tests did not show clinically relevant abnormalities. All participants refrained from alcohol consumption as well as other medication before PET imaging. After careful screening, 34 participants were enrolled into this study from 2012-12-04 to 2017-05-31 at the Department of Psychiatry and Psychotherapy, Medical University of Vienna. Seven subjects did not enter analysis due to poor data quality, leaving 27 healthy participants (*mean age: 26.22, SD: 2.36, ranging from 22 to 31; 12 females*) for final data analysis.

2.2. [^{11}C]-(+)-PHNO positron emission tomography imaging

Radiosynthesis of [^{11}C]-(+)-PHNO has been described in detail elsewhere (Rami-Mark et al., 2013). PET imaging was performed using a GE Advance scanner (General Electric Medical Systems, Milwaukee, WI, USA). After injection of 315.7 MBq ± 76.2 [^{11}C]-(+)-PHNO, emission data were obtained over 90 min. Reconstruction of raw data was performed by filtered-back projection to return dynamic images with 15 one min frames and 15 five min frames. The software AFNI (AFNI_17.3.06, NIMH, Bethesda, MD, USA) was used for frame-wise motion correction and co-registration of average PET images to T1-weighted magnetic resonance imaging (MRI) data. MRI images were normalized to the Montreal Neurological Institute (MNI) space and transformation matrices were used for normalization of PET images. Decay-corrected time activity curves were extracted from dynamic PET images using regions of interest (ROIs) from the high-resolution probabilistic in vivo atlas of subcortical nuclei by Pauli et al. (Pauli et al., 2018), which includes the majority of relevant subcortical structures. [^{11}C]-(+)-PHNO BP_{ND} values were calculated using the simplified reference tissue model 2 (SRTM2) (Ginovart et al., 2007; Wu and Carson, 2002) as implemented in PMOD software (Version 3.6; PMOD Technologies Ltd, Zurich, Switzerland). The cerebellum was used as a reference region, since it is virtually devoid of dopamine $D_{2/3}$ receptors (Camps et al., 1989; Hall et al., 1996; Levant, 1998).

To test the reliability of local imaging procedures, five male healthy subjects (*mean age: 26, SD: 1.1*) underwent two [^{11}C]-(+)-PHNO PET scans at least one weak apart. Data were preprocessed and analyzed as described above. Subsequently, test-retest reliability was assessed using Pearson Interclass Correlation Coefficients (Liljequist et al., 2019).

2.3. Magnetic resonance imaging

MRI measurements were conducted on an Achieva 3.0 T (Philips Medical Systems, Best, The Netherlands) or a Magnetom Skyra 3.0 T scanner (Siemens Healthineers, Erlangen, Germany) with a spatial resolution of 0.9 × 0.9 × 1.1 mm using comparable acquisition protocols.

2.4. Whole-brain gene expression

The AHBA comprises up to 3702 microarray samples with a voxel size of 2 mm across the whole brain from six healthy subjects (*mean age: 42.5, SD: 13.4; one female*). A detailed summary of mRNA data acquisition and processing was published upon creation of the atlas (Hawrylycz et al., 2012; Shen et al., 2012). Within the AHBA, gene expression values (log2) of the D_2 and D_3 receptor are represented in MNI space by 5 and 7 probes, respectively. Out of all available probes for both receptors, the median mRNA values were included for further analyses. DRD2 and DRD3 gene expression data were obtained only for subcortical regions in order to perform region-wise analyses in ROIs that show sufficiently reliable [^{11}C]-(+)-PHNO BP_{ND} and to avoid bias due to disparate gene expression levels between cortical and subcortical regions (Chen et al., 2016; Kirsch and Chechik, 2016). Due to the unbalanced sex distribution of the AHBA, differences in gene expression were not analyzed separately for male and female brain donors.

Original gene expression data were averaged within ROIs and subsequently combined into a brain template, including mRNA expression from all AHBA donor brains. In case of identical sample coordinates within the resulting brain template, overlapping mRNA expression values were averaged beforehand within these voxels. Despite widespread anatomical coverage, data prediction from the AHBA is potentially hampered in small subcortical regions due to sparse anatomical sampling. For compensating this sampling bias, we additionally obtained interpolated predictions of gene expression for D_2 and D_3 receptors from corresponding transcriptome maps recently published by Gryglewski et al. (Gryglewski et al., 2018). Except for the receptors investigated in this study, further whole-brain transcriptome maps based on Gaussian process regression are available online at www.meduniwien.ac.at/neuroimaging/mRNA.html for a total of 18,686 genes.

Table 1
[^{11}C]-(+)-PHNO binding potentials obtained from 27 healthy subjects and mRNA expression from the Allen Human Brain Atlas are provided within regions-of-interest labeled according to Pauli et al. (Pauli et al., 2018). Gene expression values were extracted from interpolated transcriptome maps provided by Gryglewski et al. (Gryglewski et al., 2018).

ROI (Pauli)	[^{11}C]-(+)-PHNO BP_{ND}	D_2 rec. mRNA (log2)	D_3 rec. mRNA (log2)
CAU	1.00 ± 0.16	5.19 ± 0.50	3.85 ± 1.06
EA	1.61 ± 0.25	4.49 ± 0.20	3.02 ± 0.69
GP ext.	2.45 ± 0.35	4.45 ± 0.22	2.55 ± 0.59
GP int.	2.12 ± 0.41	4.23 ± 0.10	2.19 ± 0.33
HN	0.11 ± 0.05	4.30 ± 0.12	1.83 ± 0.12
Hypo	0.91 ± 0.16	4.49 ± 0.08	1.97 ± 0.28
NAc	2.48 ± 0.31	4.40 ± 0.67	3.77 ± 1.46
PPN	0.49 ± 0.10	4.86 ± 0.12	2.09 ± 0.06
PUT	1.71 ± 0.22	4.85 ± 0.50	3.13 ± 0.95
RN	0.38 ± 0.08	4.75 ± 0.09	2.17 ± 0.08
SNC	0.59 ± 0.11	4.99 ± 0.40	2.12 ± 0.06
SNR	0.62 ± 0.11	5.00 ± 0.05	2.12 ± 0.07
VP	3.14 ± 0.45	4.49 ± 0.12	3.95 ± 0.74
VT	0.56 ± 0.12	4.83 ± 0.13	2.07 ± 0.04

Legend: ROI: region-of-interest, Pauli: Pauli atlas, CAU: caudate nucleus, EA: extended amygdala, GP ext.: globus pallidus externus, GP int.: globus pallidus internus, HN: habenular nuclei, Hypo: hypothalamus, NAc: nucleus accumbens, PPN: parabrachial pigmented nucleus, PUT: putamen, RN: red nucleus, SNC: substantia nigra pars compacta, SNR: substantia nigra pars reticulata, VP: ventral pallidum, VT: ventral tegmentum.

2.5. Statistical analysis

Statistical analysis was performed using R (Version 3.1.1, http://www.R-project.org/). Group-averaged [^{11}C]-(+)-PHNO BP_{ND} values were used for correlation analyses with gene expression data. Original mRNA data from the AHBA as well as interpolated expression values from whole-brain transcriptome maps were extracted within corresponding ROIs to allow further correlation with imaging parameters. Variability of PET and mRNA data within each brain region was evaluated in terms of mean and standard deviation values. The brain atlas by Pauli et al. (Pauli et al., 2018) was used both for brain parcellation of imaging data as well as for region-wise extraction of gene expression values. To evaluate possible influences of sex, [^{11}C]-(+)-PHNO BP_{ND} values were also extracted for female and male subjects separately. Additionally, the relationship between radiotracer binding and age was examined to rule out a potentially confounding effect, since there is conflicting literature on this topic (Nakajima et al., 2015, Matuskey et al., 2016).

To unravel information about binding to D_2 and D_3 receptors from [^{11}C]-(+)-PHNO data, radioligand BP_{ND} were compared with gene expression values by means of Pearson Product Moment correlation coefficients after testing for normality using Shapiro-Wilk tests. Additionally, associations were assessed by means of Spearman's correlation coefficients. Binding of [^{11}C]-(+)-PHNO to D_2^{low} receptors was considered negligible, leaving D_2^{high} and D_3 fractions of [^{11}C]-(+)-PHNO BP_{ND} for statistical analysis. Given the mixed $D_{2/3}$ signal of [^{11}C]-(+)-PHNO with a stronger affinity to D_3 receptors, we alternatively estimated the D_3 ratio (D_3% mRNA) based on gene expression data. D_3% mRNA was calculated from the ratio between DRD3 and the sum of DRD2 and DRD3 expression values (D_3% mRNA: $D_3/(D_2+D_3)^*100$).

3. Results

[^{11}C]-(+)-PHNO BP_{ND} values showed the expected binding pattern described earlier (Willeit et al., 2008). Briefly, high radiotracer enrichment was found in the ventral pallidum (BP_{ND}: 3.14 ± 0.45), nucleus accumbens (BP_{ND}: 2.48 ± 0.31), as well as globus pallidus externus (BP_{ND}: 2.45 ± 0.35) and internus (BP_{ND}: 2.12 ± 0.41). Likewise, mRNA levels varied across these brain regions with comparable expression values between original AHBA and interpolated transcriptome data (see Table 1 and Fig. 1). There was no significant relationship between [^{11}C]-(+)-PHNO BP_{ND} and age in any of the analyzed regions ($p > 0.05$).

Data reliability in the test-retest sample according to Pearson interclass correlation coefficients was excellent (> 0.9) for the caudate and the putamen, good (> 0.75) for the extended amygdala, globus pallidus, habenular nuclei, hypothalamus, mammillary nucleus, nucleus accumbens, and moderate (> 0.5) for the parabrachial pigmented nucleus, red nucleus, substantia nigra compacta et reticulata, subthalamic nucleus, ventral pallidum and ventral tegmentum. Remarkably, no regions showed poor reliability (< 0.5).

Associations of gene expression data with [^{11}C]-(+)-PHNO BP_{ND} were primarily evaluated by means of Pearson Product Moment correlation coefficients. Correlation analyses using interpolated mRNA data yielded similar results for all analyses compared to the original AHBA data. As hypothesized, DRD3 expression data showed a strong correlation with [^{11}C]-(+)-PHNO BP_{ND} across the whole brain (interpolated: $r = 0.69$, $p = 0.006$; original data: $r = 0.71$, $p < 0.01$). Brain areas rich in D_3 receptors showed both high radioligand binding and high mRNA expression (see Fig. 2). In contrast, DRD2 expression showed no significant correlation with [^{11}C]-(+)-PHNO BP_{ND} values (interpolated: $r = -0.46$, $p = 0.1$; original data: $r = 0.11$, $p = 0.68$). A significant correlation between [^{11}C]-(+)-PHNO BP_{ND} and D_3% mRNA was also observed (interpolated: $r = 0.8$, $p < 0.01$; original data: $r = 0.51$, $p = 0.04$), supporting the D_3 binding preference of [^{11}C]-(+)-PHNO (see Fig. 3). The linear associations were subsequently confirmed by Spearman's rank correlation coefficients, which yielded similar results (interpolated: D_3 rho = 0.78, $p = 0.001$; D_2 rho = -0.31, $p = 0.28$; original data: D_3 rho = 0.68, $p = 0.004$; D_2 rho = 0.14, $p = 0.60$). Likewise, separate analyses for female and male subjects yielded comparable results, both for the D_3 (female interpolated: $r = 0.7$, $p = 0.005$; male interpolated: $r = 0.71$, $p = 0.004$) and D_2 receptor (female interpolated: $r = -0.47$, $p = 0.09$; male interpolated: $r = -0.43$, $p = 0.13$).

4. Discussion

In this study, we integrated high-resolution gene expression maps from the AHBA open-source database with specific molecular information on dopamine receptor binding acquired with PET imaging. Our main finding is that [^{11}C]-(+)-PHNO BP_{ND} values were strongly correlated with D_3 receptor mRNA expression levels. In contrast, we failed to observe a significant correlation for the D_2 receptor. In a next step, we intended to mimic the mixed $D_{2/3}$ receptor signal of [^{11}C]-(+)-PHNO by calculating the D_3 mRNA ratio from the sum of DRD3 and DRD2 expression values. Likewise, the significant correlations reflect a linear relationship between mRNA expression and agonist radioligand binding that exists with D_3 but not D_2 receptors. Displaying comparable in

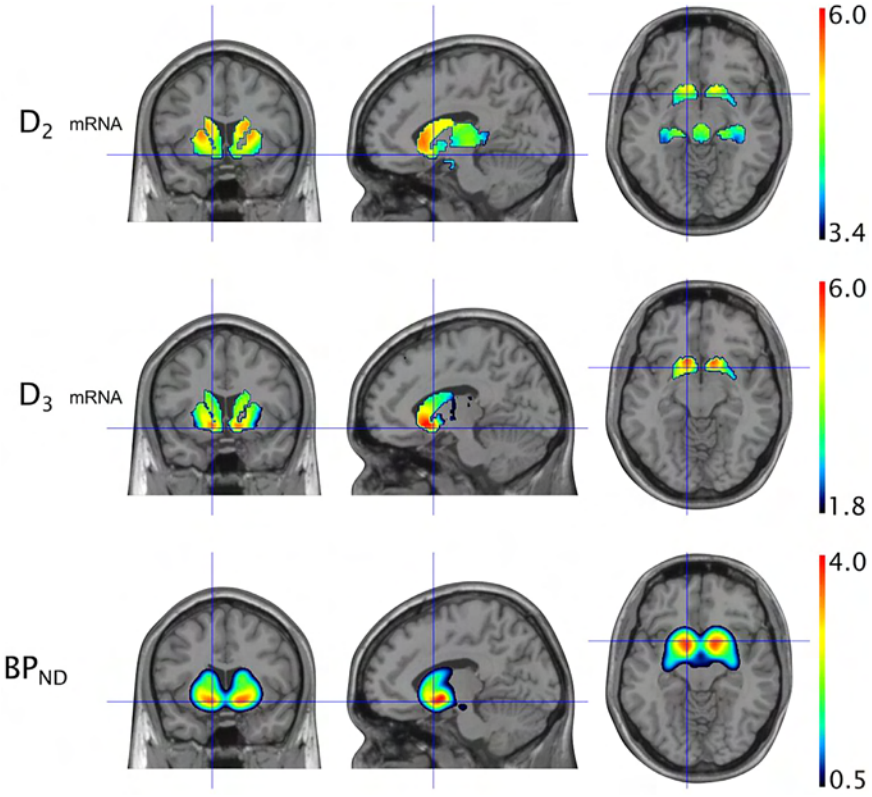

Fig. 1. Statistical parametric maps displaying distributions of dopamine D_2 and D_3 receptors. Interpolated gene expression patterns (log2) according to Gryglewski et al. (Gryglewski et al., 2018) are depicted in MNI space (x = −12, y = 10, z = −10) for both dopamine receptors in the upper two panels, while [^{11}C]-(+)-PHNO binding (BP_{ND}) is provided in the lowest panel.

vitro affinity for D_2^{high} and D_3 (Seeman et al., 1993), [^{11}C]-(+)-PHNO, in vivo, provides a mixed signal composed of binding to D_2 receptors in high affinity states and D_3 receptors (Graff-Guerrero et al., 2010; Rabiner et al., 2009; Searle et al., 2010; Tziortzi et al., 2011). While strong correlations with D_3 mRNA levels indicate a direct relationship between D_3 protein expression and [^{11}C]-(+)-PHNO BP_{ND} values, the failure to observe such a relationship with D_2 mRNA levels supports the notion that G-protein-dependent variations in affinity states are more relevant for D_2 than for D_3 receptors (Sokoloff et al., 1992). Although alternative explanations such as posttranslational modifications, trafficking processes or a simple lack of power need to be considered, our data highlight the relevance of the two-state model for dopamine receptor functioning in the living human brain. Thereby, the affinity states of D_2 receptors depend on G-protein coupling (George et al., 1985), which explains the weak correlation for [^{11}C]-(+)-PHNO BP_{ND} and overall D_2 gene expression including a large proportion of D_2^{low} receptors.

In contrast to previous studies evaluating the role of mRNA expression patterns on PET binding potentials for serotonergic targets (Komorowski et al., 2017; Veronese et al., 2016), we now analyzed binding of a radiotracer that is well established in imaging of the dopamine system. Thereby, the role of D_2 and D_3 receptors in neuropsychiatric disorders and alterations of dopamine signaling, which is modified by cortical and other upstream regions, can be assessed by PET imaging using [^{11}C]-(+)-PHNO. Our study shows how open-source mRNA expression data can be utilized to gain further information about specific protein targets in humans, surrogating the in vivo topological distribution. However, a closer investigation in regard to radiotracer binding and the molecular effects of gene variants is necessary to fully understand regional protein biosynthesis of dopamine receptors.

In general, differing correlation coefficients between both dopamine receptors might arise from epitranscriptomic modifications or alternating in vivo conformational states (Mauer and Jaffrey, 2018). E.g. analyses for D_2 receptors, which exist in high and low affinity states, were complicated by their varying affinity to [^{11}C]-(+)-PHNO. To overcome this methodological limitation, human proteomic data comprising functional genetic variants as well as information on transcriptional, translational and posttranslational mechanisms are needed. Yet, when considering potential epitranscriptomic processes of dopaminergic receptors (Araki et al., 2007; Flagel et al., 2016), the noncongruent findings between both analyzed dopamine receptors indeed appear to originate from receptor-specific binding preferences of [^{11}C]-(+)-PHNO rather than differing mRNA modifications. The results of this study are, however, hampered by the fact that post-mortem mRNA expression data from the AHBA were obtained in a small number of subjects including limited transcriptome information from only one female donor and one hemisphere in four out of six sampled brains (Hawrylycz et al., 2012). Upon creation of the atlas, ubiquitous coverage of gene expression samples across the entire brain was prioritized over a balanced donor distribution. Although separate association analyses with regard to sex, age, or ancestry were not possible for mRNA data, these disadvantages appear negligible. Notably, the relationship between male and female [^{11}C]-(+)PHNO BP_{ND} and mRNA expression data didn't show significant differences when analyzed separately. Regarding other potential confounders, Matuskey et al. have described a decline of the densities of dopamine receptors with age (Matuskey et al., 2016). While this predominantly affected D_2 receptor availability rather than D_3 receptors, other authors did not oberve age-associated changes in the dopamine system (Nakajima et al., 2015). Even though only participants aged from 22 to 31 were included in this study, the fact that we didn't find a relationship between age and [^{11}C]-(+)PHNO BP_{ND} indicated a rather insignificant role of age for subsequent correlation analyses.

Gene expression values based on microarray data often suffer from background and cross-hybridization disturbances (Maier et al., 2009), complicating the assumption of comparable absolute mRNA values between both dopamine receptors. Still, possible differences in absolute gene expression values between both receptors didn't impact on the respective correlation analyses with [^{11}C]-(+)-PHNO BP_{ND} that were performed for each receptor separately. Beside these limitations, we still re-

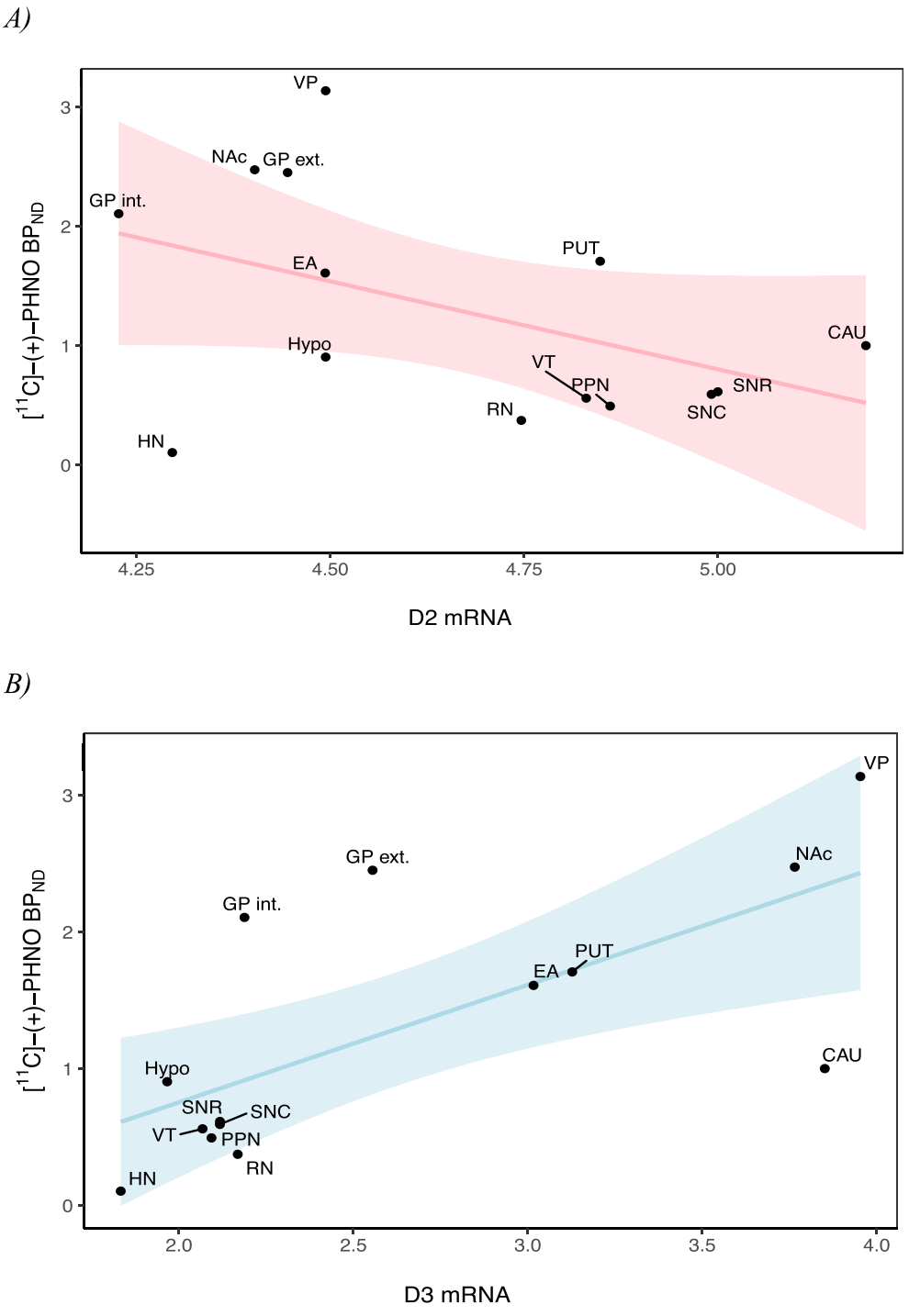

Fig. 2. Relationship between [^{11}C]-(+)-PHNO BP_{ND} and interpolated mRNA data (log2) for A) the D_2 receptor (t = -1.79, df = 12, r = -0.46, p = 0.1) and B) the D_3 receptor (t = 3.30, df = 12, r = 0.69, p = 0.006). Regions-of-interest were labeled according to Pauli et al. (Pauli et al., 2018).
Legend: ROI: region-of-interest, Pauli: Pauli atlas, CAU: caudate nucleus, EA: extended amygdala, GP ext.: globus pallidus externus, GP int.: globus pallidus internus, HN: habenular nuclei, Hypo: hypothalamus, NAc: nucleus accumbens, PPN: parabrachial pigmented nucleus, PUT: putamen, RN: red nucleus, SNC: substantia nigra pars compacta, SNR: substantia nigra pars reticulata, VP: ventral pallidum, VT: ventral tegmentum.

gard the AHBA as an extremely valuable data source for comprehensive neuroimaging studies. To compensate for the incomplete gene expression coverage of the brain due to sparse sampling of the AHBA within several brain regions, we have analyzed interpolated gene expression data provided by Gryglewski et al. (Gryglewski et al., 2018) in addition to the original data. Interpolated expression values of dopaminergic receptors were thereby approximated with a high spatial resolution across the whole brain. Aside from that, there is still ongoing controversy regarding the selection of probes included within the AHBA. Each method, e.g. performing separate analyses for each probe, or averaging all available probes, has its advantages and disadvantages (Arnatkevičiūtė et al., 2019; Komorowski et al., 2017; Veronese et al., 2016). By selecting the median gene expression value within each brain region, we minimized possible bias on our analysis introduced by insensitive probes from the AHBA, yielding representative gene expression values within all ROIs. Considering the interpolated data by Gryglewski et al. (Gryglewski et al., 2018), probes were selected by means of a step-wise variogram modeling approach, eliminating the least sensitive probes before calculating a mean value for each mRNA sample.

In sum, we elucidated the relationship between gene expression and the mixed imaging signal of [^{11}C]-(+)-PHNO. The results of this study also indicate unique transcriptional processes for different brain regions, leading to characteristic distribution patterns of the D_2 and D_3 dopamine receptor with a high variability between brain regions. Notably, neu-

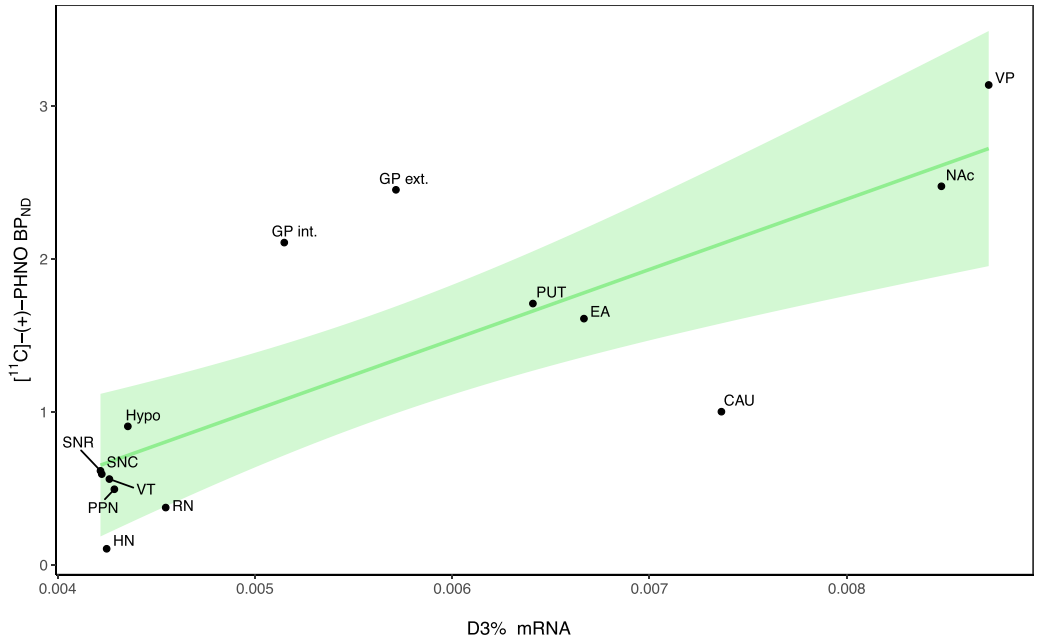

Fig. 3. Relationship between radiotracer binding and the D3 ratio based on interpolated gene expression data (log2) from both receptors (D_3% mRNA: $D_3/(D_2+D_3)$*100), approximating the mixed [^{11}C]-(+)-PHNO signal (t = 4.65, df = 12, r = 0.8, p < 0.01). Regions-of-interest were labeled according to Pauli et al. (Pauli et al., 2018).

Legend: ROI: region-of-interest, Pauli: Pauli atlas, CAU: caudate nucleus, EA: extended amygdala, GP ext.: globus pallidus externus, GP int.: globus pallidus internus, HN: habenular nuclei, Hypo: hypothalamus, NAc: nucleus accumbens, PPN: parabrachial pigmented nucleus, PUT: putamen, RN: red nucleus, SNC: substantia nigra pars compacta, SNR: substantia nigra pars reticulata, VP: ventral pallidum, VT: ventral tegmentum.

roimaging studies significantly benefit from gene expression information, especially for targets that lack sufficiently specific radiotracers in humans. Furthering this knowledge might enhance the definition of new molecular targets for the treatment of neuropsychiatric disorders.

5. Conclusion

This study supports evidence of differing binding properties of [^{11}C]-(+)-PHNO to D_2 and D_3 dopamine receptors in different brain regions. According to our data, regional dopamine D_3 receptor mRNA expression is a more relevant determinant of [^{11}C]-(+)-PHNO binding than expression of the D_2 receptor, whose affinity states depend to a greater degree on G-protein coupling. Overall, combining in vivo imaging and post-mortem gene expression data contributes to the understanding of the [^{11}C]-(+)-PHNO PET signal from a new perspective.

Declaration of Competing Interest

Without relevance to this work, Matthäus Willeit declares to having received speaker honoraria and consulting fees from Janssen-Cilag Pharma GmbH, Austria. Wolfgang Wadsak declares to having received speaker honoraria from GE Healthcare, research grants from Ipsen Pharma, Eckert-Ziegler AG, Scintomics and ITG. He is a part time employee of CBmed Ltd (Center for Biomarker Research in Medicine, Graz, Austria). Marcus Hacker received consulting fees and/or honoraria from Bayer Healthcare BMS, Eli Lilly, EZAG, GE Healthcare, Ipsen, ITM, Janssen, Roche, Siemens Healthineers. Rupert Lanzenberger received travel grants and/or conference speaker honoraria within the last three years from Bruker BioSpin MR, Heel, and support from Siemens Healthcare regarding clinical research using PET/MR. Siegfried Kasper received grants/research support, consulting fees and/or honoraria within the last three years from Angelini, AOP Orphan Pharmaceuticals AG, Celegne GmbH, Eli Lilly, Janssen-Cilag Pharma GmbH, KRKA-Pharma, Lundbeck A/S, Mundipharma, Neuraxpharm, Pfizer, Sanofi, Schwabe, Servier, Shire, Sumitomo Dainippon Pharma Co. Ltd. and Takeda. Arkadiusz Komorowski, Ana Weidenauer, Martin Bauer, Ulrich Sauerzopf, Matej Murgaš, Markus Mitterhauser, and Nicole Praschak-Rieder have no conflicts of interest to declare.

CRediT authorship contribution statement

Arkadiusz Komorowski: Conceptualization, Writing - original draft, Investigation. **Ana Weidenauer:** Conceptualization, Writing - original draft, Formal analysis. **Matej Murgaš:** Data curation, Methodology, Software, Visualization. **Ulrich Sauerzopf:** Data curation, Software, Writing - review & editing. **Wolfgang Wadsak:** Resources, Validation. **Markus Mitterhauser:** Resources, Validation. **Martin Bauer:** Resources, Writing - review & editing. **Marcus Hacker:** Resources. **Nicole Praschak-Rieder:** Resources. **Siegfried Kasper:** Resources, Supervision, Writing - review & editing. **Rupert Lanzenberger:** Project administration, Funding acquisition, Resources, Supervision, Writing - review & editing. **Matthäus Willeit:** Project administration, Funding acquisition, Resources, Supervision, Writing - review & editing.

Acknowledgements

We thank the diploma students of the Neuroimaging Lab (NIL) as well as the staff at the Department of Psychiatry and Psychotherapy and the Department of Biomedical Imaging and Image-guided Therapy, Division of Nuclear Medicine for clinical, scientific, administrative, and technical support, respectively. Furthermore, we would like to thank Gregor Gryglewski for making parametric voxel-wise RNA data available to us.

Funding

This study was funded by the Austrian Science Fund FWF [Grant No. P23585-B09, granted to M.W.; Grant No. KLI-516 granted to R.L.; Doc.funds No. DOC 33-B27, granted to M.M.], the Anniversary Fund of the Austrian National Bank [Grant No. 16723, granted to M.W.],

the Medical Scientific Fund of the Mayor of Vienna (Medizinisch-Wissenschaftlicher Fonds des Bürgermeisters der Bundeshauptstadt Wien) [Grant No. 15189, granted to M.W.], and the Vienna Science and Technology Fund (WWTF) [Grant No. CS15-033, granted to M.W.]. The funding sources had no further role in the study design, or the collection, analysis and interpretation of data.

Data and code availability statement

Positron emission tomography data generated during this study are available from the corresponding author upon reasonable request on condition of a formal data sharing agreement. Gene expression data can be obtained from the Allen Human Brain Atlas online framework (https://human.brain-map.org/) and whole-brain transcriptome maps are available from the Neuroimaging Labs (NIL) (www.meduniwien.ac.at/neuroimaging/mRNA.html). The codes that were included in this study are available from the corresponding author upon reasonable request.

References

Araki, K.Y., Sims, J.R., Bhide, P.G., 2007. Dopamine receptor mRNA and protein expression in the mouse corpus striatum and cerebral cortex during pre- and postnatal development. Brain Res. 1156, 31–45.

Arnatkevičiūtė, A., Fulcher, B.D., Fornito, A., 2019. A practical guide to linking brain-wide gene expression and neuroimaging data. Neuroimage 189, 353–367.

Beaulieu, J.M., Gainetdinov, R.R., 2011. The physiology, signaling, and pharmacology of dopamine receptors. Pharmacol Rev 63, 182–217.

Boileau, I., Nakajima, S., Payer, D., 2015. Imaging the D3 dopamine receptor across behavioral and drug addictions: positron emission tomography studies with [(11)C]-(+)-PHNO. Eur Neuropsychopharmacol 25, 1410–1420.

Boileau, I., Payer, D., Houle, S., Behzadi, A., Rusjan, P.M., Tong, J., Wilkins, D., Selby, P., George, T.P., Zack, M., Furukawa, Y., McCluskey, T., Wilson, A.A., Kish, S.J., 2012. Higher binding of the dopamine D3 receptor-preferring ligand [11C]-(+)-propyl-hexahydro-naphtho-oxazin in methamphetamine polydrug users: a positron emission tomography study. J. Neurosci. 32, 1353–1359.

Brown, D.J., Luthra, S.K., Brady, F., Prenant, C., Dijkstra, D., Wikström, H., Brooks, D., 1997. Labeling of the D2 agonist -(+)-PHNO using [^{11}C]-Propionyl chloride. In: XIIth Int. Symp. Radiopharmaceutical Chemistry, Uppsala, Sweden. Wiley, Chichester, U.K, pp. 565–566.

Burt, J.B., Demirtas, M., Eckner, W.J., et al., 2018. Hierarchy of transcriptomic specialization across human cortex captured by myelin map topography. Nat Neurosci 21, 1251–1259. doi:10.1038/s41593-018-0195-0.

Camps, M., Cortes, R., Gueye, B., Probst, A., Palacios, J.M., 1989. Dopamine receptors in human brain: autoradiographic distribution of D2 sites. Neuroscience 28, 275–290.

Chen, L., Chu, C., Zhang, Y.H., Zhu, C., Kong, X., Huang, T., Cai, Y.D., 2016. Analysis of gene expression profiles in the human brain stem, cerebellum and cerebral cortex. PLoS One 11, e0159395.

Flagel, S.B., Chaudhury, S., Waselus, M., Kelly, R., Sewani, S., Clinton, S.M., Thompson, R.C., Watson Jr., S.J., Akil, H., 2016. Genetic background and epigenetic modifications in the core of the nucleus accumbens predict addiction-like behavior in a rat model. Proc. Natl. Acad. Sci. USA 113, E2861–E2870.

Gallezot, J.D., Beaver, J.D., Gunn, R.N., Nabulsi, N., Weinzimmer, D., Singhal, T., Slifstein, M., Fowles, K., Ding, Y.S., Huang, Y., Laruelle, M., Carson, R.E., Rabiner, E.A., 2012. Affinity and selectivity of [(1)(1)C]-(+)-PHNO for the D3 and D2 receptors in the rhesus monkey brain in vivo. Synapse 66, 489–500.

George, S.R., Watanabe, M., Di Paolo, T., Falardeau, P., Labrie, F., Seeman, P., 1985. The functional state of the dopamine receptor in the anterior pituitary is in the high affinity form. Endocrinology 117, 690–697.

Ginovart, N., Galineau, L., Willeit, M., Mizrahi, R., Bloomfield, P.M., Seeman, P., Houle, S., Kapur, S., Wilson, A.A., 2006. Binding characteristics and sensitivity to endogenous dopamine of [11C]-(+)-PHNO, a new agonist radiotracer for imaging the high-affinity state of D2 receptors in vivo using positron emission tomography. J. Neurochem. 97, 1089–1103.

Ginovart, N., Willeit, M., Rusjan, P., Graff, A., Bloomfield, P.M., Houle, S., Kapur, S., Wilson, A.A., 2007. Positron emission tomography quantification of [11C]-(+)-PHNO binding in the human brain. J. Cereb. Blood Flow Metab. 27, 857–871.

Goel, P., Kuceyeski, A., LoCastro, E., Raj, A., 2014. Spatial patterns of genome-wide expression profiles reflect anatomic and fiber connectivity architecture of healthy human brain. Hum. Brain Mapp. 35, 4204–4218.

Graff-Guerrero, A., Mizrahi, R., Agid, O., Marcon, H., Barsoum, P., Rusjan, P., Wilson, A.A., Zipursky, R., Kapur, S., 2009. The dopamine D2 receptors in high-affinity state and D3 receptors in schizophrenia: a clinical [11C]-(+)-PHNO PET study. Neuropsychopharmacology 34, 1078–1086.

Graff-Guerrero, A., Redden, L., Abi-Saab, W., Katz, D.A., Houle, S., Barsoum, P., Bhathena, A., Palaparthy, R., Saltarelli, M.D., Kapur, S., 2010. Blockade of [11C](+)-PHNO binding in human subjects by the dopamine D3 receptor antagonist ABT-925. Int. J. Neuropsychopharmacol. 13, 273–287.

Gryglewski, G., Seiger, R., James, G.M., Godbersen, G.M., Komorowski, A., Unterholzner, J., Michenthaler, P., Hahn, A., Wadsak, W., Mitterhauser, M., Kasper, S., Lanzenberger, R., 2018. Spatial analysis and high resolution mapping of the human whole-brain transcriptome for integrative analysis in neuroimaging. Neuroimage 176, 259–267.

Hall, H., Farde, L., Halldin, C., Hurd, Y.L., Pauli, S., Sedvall, G., 1996. Autoradiographic localization of extrastriatal D2-dopamine receptors in the human brain using [125I]epidepride. Synapse 23, 115–123.

Hawrylycz, M.J., Lein, E.S., Guillozet-Bongaarts, A.L., Shen, E.H., Ng, L., Miller, J.A., van de Lagemaat, L.N., Smith, K.A., Ebbert, A., Riley, Z.L., Abajian, C., Beckmann, C.F., Bernard, A., Bertagnolli, D., Boe, A.F., Cartagena, P.M., Chakravarty, M.M., Chapin, M., Chong, J., Dalley, R.A., David Daly, B., Dang, C., Datta, S., Dee, N., Dolbeare, T.A., Faber, V., Feng, D., Fowler, D.R., Goldy, J., Gregor, B.W., Haradon, Z., Haynor, D.R., Hohmann, J.G., Horvath, S., Howard, R.E., Jeromin, A., Jochim, J.M., Kinnunen, M., Lau, C., Lazarz, E.T., Lee, C., Lemon, T.A., Li, L., Li, Y., Morris, J.A., Overly, C.C., Parker, P.D., Parry, S.E., Reding, M., Royall, J.J., Schulkin, J., Sequeira, P.A., Slaughterbeck, C.R., Smith, S.C., Sodt, A.J., Sunkin, S.M., Swanson, B.E., Vawter, M.P., Williams, D., Wohnoutka, P., Zielke, H.R., Geschwind, D.H., Hof, P.R., Smith, S.M., Koch, C., Grant, S.G.N., Jones, A.R., 2012. An anatomically comprehensive atlas of the adult human brain transcriptome. Nature 489, 391–399.

Jensen, J., Smith, A.J., Willeit, M., Crawley, A.P., Mikulis, D.J., Vitcu, I., Kapur, S., 2007. Separate brain regions code for salience vs. valence during reward prediction in humans. Hum Brain Mapp 28, 294–302.

Kirsch, L., Chechik, G., 2016. On expression patterns and developmental origin of human brain regions. PLoS Comput. Biol. 12, e1005064.

Komorowski, A., James, G.M., Philippe, C., Gryglewski, G., Bauer, A., Hienert, M., Spies, M., Kautzky, A., Vanicek, T., Hahn, A., Traub-Weidinger, T., Winkler, D., Wadsak, W., Mitterhauser, M., Hacker, M., Kasper, S., Lanzenberger, R., 2017. Association of protein distribution and gene expression revealed by PET and post-mortem quantification in the serotonergic system of the human brain. Cereb Cortex 27, 117–130.

Levant, B., 1998. Differential distribution of D3 dopamine receptors in the brains of several mammalian species. Brain Res 800, 269–274.

Liljequist, D., Elfving, B., Skavberg Roaldsen, K., 2019. Intraclass correlation - a discussion and demonstration of basic features. PLoS One 14, e0219854.

Maier, T., Guell, M., Serrano, L., 2009. Correlation of mRNA and protein in complex biological samples. FEBS Lett. 583, 3966–3973.

Matuskey, D., Worhunksy, P., Correa, E., Pittman, B., Gallezot, J.D., Nabulsi, N., Ropchan, J., Sreeram, V., Gudepu, R., Gaiser, E., Cosgrove, K., Ding, Y.S., Potenza, M.N., Huang, Y., Malison, R.T., Carson, R.E., 2016. Age-related changes in binding of the D2/3 receptor radioligand [(11)C](+)PHNO in healthy volunteers. Neuroimage 130, 241–247.

Mauer, J., Jaffrey, S.R., 2018. FTO, m(6) Am, and the hypothesis of reversible epitranscriptomic mRNA modifications. FEBS Lett. 592, 2012–2022.

Mizrahi, R., Addington, J., Rusjan, P.M., Suridjan, I., Ng, A., Boileau, I., Pruessner, J.C., Remington, G., Houle, S., Wilson, A.A., 2012. Increased stress-induced dopamine release in psychosis. Biol Psychiatry 71, 561–567.

Mizrahi, R., Agid, O., Borlido, C., Suridjan, I., Rusjan, P., Houle, S., Remington, G., Wilson, A.A., Kapur, S., 2011. Effects of antipsychotics on D3 receptors: a clinical PET study in first episode antipsychotic naive patients with schizophrenia using [11C]-(+)-PHNO. Schizophr Res. 131, 63–68.

Mizrahi, R., Kenk, M., Suridjan, I., Boileau, I., George, T.P., McKenzie, K., Wilson, A.A., Houle, S., Rusjan, P., 2014. Stress-induced dopamine response in subjects at clinical high risk for schizophrenia with and without concurrent cannabis use. Neuropsychopharmacology 39, 1479–1489.

Nakajima, S., Caravaggio, F., Boileau, I., Chung, J.K., Plitman, E., Gerretsen, P., Wilson, A.A., Houle, S., Mamo, D.C., Graff-Guerrero, A., 2015. Lack of age-dependent decrease in dopamine D3 receptor availability: a [(11)C]-(+)-PHNO and [(11)C]-raclopride positron emission tomography study. J. Cereb. Blood Flow Metab. 35, 1812–1818.

Nobrega, J.N., Seeman, P., 1994. Dopamine D2 receptors mapped in rat brain with [3H](+)PHNO. Synapse 17, 167–172.

Pauli, W.M., Nili, A.N., Tyszka, J.M., 2018. A high-resolution probabilistic in vivo atlas of human subcortical brain nuclei. Sci Data 5, 180063.

Payer, D.E., Behzadi, A., Kish, S.J., Houle, S., Wilson, A.A., Rusjan, P.M., Tong, J., Selby, P., George, T.P., McCluskey, T., Boileau, I., 2014. Heightened D3 dopamine receptor levels in cocaine dependence and contributions to the addiction behavioral phenotype: a positron emission tomography study with [11C]-+-PHNO. Neuropsychopharmacology 39, 311–318.

Rabiner, E.A., Slifstein, M., Nobrega, J., Plisson, C., Huiban, M., Raymond, R., Diwan, M., Wilson, A.A., McCormick, P., Gentile, G., Gunn, R.N., Laruelle, M.A., 2009. In vivo quantification of regional dopamine-D3 receptor binding potential of (+)-PHNO: Studies in non-human primates and transgenic mice. Synapse 63, 782–793.

Rami-Mark, C., Ungersboeck, J., Haeusler, D., Nics, L., Philippe, C., Mitterhauser, M., Willeit, M., Lanzenberger, R., Karanikas, G., Wadsak, W., 2013. Reliable set-up for in-loop 11C-carboxylations using Grignard reactions for the preparation of [carbonyl-11C] WAY-100635 and [11C]-(+)-PHNO. Applied Radiation and Isotopes 82, 75–80.

Richiardi, J., Altmann, A., Milazzo, A.C., Chang, C., Chakravarty, M.M., Banaschewski, T., Barker, G.J., Bokde, A.L., Bromberg, U., Buchel, C., Conrod, P., Fauth-Buhler, M., Flor, H., Frouin, V., Gallinat, J., Garavan, H., Gowland, P., Heinz, A., Lemaitre, H., Mann, K.F., Martinot, J.L., Nees, F., Paus, T., Pausova, Z., Rietschel, M., Robbins, T.W., Smolka, M.N., Spanagel, R., Strohle, A., Schumann, G., Hawrylycz, M., Poline, J.B., Greicius, M.D., consortium, I., 2015. BRAIN NETWORKS. Correlated gene expression supports synchronous activity in brain networks. Science 348, 1241–1244.

Rizzo, G., Veronese, M., Expert, P., Turkheimer, F.E., Bertoldo, A., 2016. MENGA: a new comprehensive tool for the integration of neuroimaging data and the allen human brain transcriptome atlas. PLoS One 11, e0148744.

Searle, G., Beaver, J.D., Comley, R.A., Bani, M., Tziortzi, A., Slifstein, M., Mugnaini, M., Griffante, C., Wilson, A.A., Merlo-Pich, E., Houle, S., Gunn, R., Rabiner, E.A., Laruelle, M., 2010. Imaging dopamine D3 receptors in the human brain with positron emission tomography, [11C]PHNO, and a selective D3 receptor antagonist. Biol. Psychiatry 68, 392–399.

Seeman, P., McCormick, P.N., Kapur, S., 2007. Increased dopamine D2(High) receptors in amphetamine-sensitized rats, measured by the agonist [(3)H](+)PHNO. Synapse 61, 263–267.

Seeman, P., Ulpian, C., Larsen, R.D., Anderson, P.S., 1993. Dopamine receptors labelled by PHNO. Synapse 14, 254–262.

Shin, J., French, L., Xu, T., Leonard, G., Perron, M., Pike, G.B., Richer, L., Veillette, S., Pausova, Z., Paus, T., 2017. Cell-specific gene-expression profiles and cortical thickness in the human brain. Cereb Cortex 1–11.

Shen, E.H., Overly, C.C., Jones, A.R., 2012. The Allen Human Brain Atlas: comprehensive gene expression mapping of the human brain. Trends in neurosciences 35 (12), 177–714.

Sokoloff, P., Andrieux, M., Besancon, R., Pilon, C., Martres, M.P., Giros, B., Schwartz, J.C., 1992. Pharmacology of human dopamine D3 receptor expressed in a mammalian cell line: comparison with D2 receptor. Eur J Pharmacol 225, 331–337.

Suridjan, I., Rusjan, P., Addington, J., Wilson, A.A., Houle, S., Mizrahi, R., 2013. Dopamine D2 and D3 binding in people at clinical high risk for schizophrenia, antipsychotic–naive patients and healthy controls while performing a cognitive task. J. Psychiatry Neurosci. 38, 98–106.

Tziortzi, A.C., Searle, G.E., Tzimopoulou, S., Salinas, C., Beaver, J.D., Jenkinson, M., Laruelle, M., Rabiner, E.A., Gunn, R.N., 2011. Imaging dopamine receptors in humans with [11C]-(+)-PHNO: dissection of D3 signal and anatomy. Neuroimage 54, 264–277.

Unterholzner, J., Gryglewski, G., Philippe, C., Seiger, R., Pichler, V., Godbersen, G.M., Berroteran-Infante, N., Murgas, M., Hahn, A., Wadsak, W., Mitterhauser, M., Kasper, S., Lanzenberger, R., 2020. Topologically guided prioritization of candidate gene transcripts coexpressed with the 5-HT1A receptor by combining in vivo PET and Allen human brain atlas data. Cereb Cortex..

Veronese, M., Zanotti-Fregonara, P., Rizzo, G., Bertoldo, A., Innis, R.B., Turkheimer, F.E., 2016. Measuring specific receptor binding of a PET radioligand in human brain without pharmacological blockade: The genomic plot. Neuroimage 130, 1–12.

Weidenauer, A., Bauer, M., Sauerzopf, U., Bartova, L., Nics, L., Pfaff, S., Philippe, C., Berroteran-Infante, N., Pichler, V., Meyer, B.M., Rabl, U., Sezen, P., Cumming, P., Stimpfl, T., Sitte, H.H., Lanzenberger, R., Mossaheb, N., Zimprich, A., Rusjan, P., Dorffner, G., Mitterhauser, M., Hacker, M., Pezawas, L., Kasper, S., Wadsak, W., Praschak-Rieder, N., Willeit, M., 2020. On the relationship of first-episode psychosis to the amphetamine-sensitized state: a dopamine D2/3 receptor agonist radioligand study. Transl Psychiatry 10, 2.

Willeit, M., Ginovart, N., Graff, A., Rusjan, P., Vitcu, I., Houle, S., Seeman, P., Wilson, A.A., Kapur, S., 2008. First human evidence of d-amphetamine induced displacement of a D2/3 agonist radioligand: A [11C]-(+)-PHNO positron emission tomography study. Neuropsychopharmacology 33, 279–289.

Willeit, M., Ginovart, N., Kapur, S., Houle, S., Hussey, D., Seeman, P., Wilson, A.A., 2006. High-affinity states of human brain dopamine D2/3 receptors imaged by the agonist [11C]-(+)-PHNO. Biol Psychiatry 59, 389–394.

Wilson, A.A., McCormick, P., Kapur, S., Willeit, M., Garcia, A., Hussey, D., Houle, S., Seeman, P., Ginovart, N., 2005. Radiosynthesis and evaluation of [11C]-(+)-4-propyl-3,4,4a,5,6,10b-hexahydro-2H-naphtho[1,2-b][1,4]oxazin-9-ol as a potential radiotracer for in vivo imaging of the dopamine D2 high-affinity state with positron emission tomography. J Med Chem 48, 4153–4160.

Worhunsky, P.D., Matuskey, D., Gallezot, J.D., Gaiser, E.C., Nabulsi, N., Angarita, G.A., Calhoun, V.D., Malison, R.T., Potenza, M.N., Carson, R.E., 2017. Regional and source-based patterns of [11C]-(+)-PHNO binding potential reveal concurrent alterations in dopamine D2 and D3 receptor availability in cocaine-use disorder. Neuroimage 148, 343–351.

Wu, Y., Carson, R.E., 2002. Noise reduction in the simplified reference tissue model for neuroreceptor functional imaging. J. Cereb. Blood Flow Metab. 22, 1440–1452.